Neuro-Oncology Advances
4(1), 1–11, 2022 | https://doi.org/10.1093/noajnl/vdac144 | Advance Access date 29 September 2022

Protein arginine methyltransferase 5 regulates SHH-subgroup medulloblastoma progression

Daniel T. Wynn, Jezabel Rodriguez-Blanco, Jun Long, Fan Yang, Chen Shen, Dennis Fei, Hsin-Yao Tang, Derek Hanson, and David J. Robbins

Department of Oncology, Lombardi Comprehensive Cancer Center, Georgetown University, Washington, DC, USA (D.T.W., C.S., D.J.R.); Department of Pediatrics, Darby Children's Research Institute, Medical University of South Carolina, Charleston, South Carolina, USA (J.R.B.); Hollings Cancer Center, Medical University of South Carolina, Charleston, South Carolina, USA (J.R.B.); The Sheila and David Fuente Graduate Program in Cancer Biology, Miller School of Medicine, University of Miami, Miami, Florida, USA (J.L., F.Y.); The Dewitt Daughtry Family Department of Surgery Molecular Oncology Lab, Miller School of Medicine, University of Miami, Miami, Florida, USA (D.F.); The Wistar Institute Proteomics and Metabolomics Facility, Philadelphia, Pennsylvania, USA (H.Y.T.); Joseph M. Sanzari Children's Hospital at Hackensack University Medical Center, Hackensack, New Jersey, USA (D.H.)

Corresponding Author: David J. Robbins, PhD, Department of Oncology, Lombardi Comprehensive Cancer Center, Georgetown University, New Research Building, Room E520A, 3970 Reservoir Road NW, Washington, DC 20057-1468, USA (dr956@georgetown.edu).

Abstract

Background. Medulloblastoma (MB) is the most common pediatric brain tumor. Although standard-of-care treatment generally results in good prognosis, many patients exhibit treatment-associated lifelong disabilities. This outcome could be improved by employing therapies targeting the molecular drivers of this cancer. Attempts to do so in the SONIC HEDGEHOG MB subgroup (SHH-MB) have largely focused on the SHH pathway's principal activator, smoothened (SMO). While inhibitors targeting SMO have shown clinical efficacy, recurrence and resistance are frequently noted, likely resulting from mutations in or downstream of SMO. Therefore, identification of novel SHH regulators that act on the pathway's terminal effectors could be used to overcome or prevent such recurrence. We hypothesized that protein arginine methyltransferase 5 (PRMT5) is one such regulator and investigated its role and potential targeting in SHH-MB.

Methods. PRMT5 expression in SHH-MB was first evaluated. Knockdown and pharmacological inhibitors of PRMT5 were used in SHH-MB sphere cultures to determine its effect on viability and SHH signaling. GLI1 arginine methylation was then characterized in primary SHH-MB tissue using LC–MS/MS. Finally, PRMT5 inhibitor efficacy was evaluated *in vivo.*

Results. PRMT5 is overexpressed in SHH-MB tissue. Furthermore, SHH-MB viability and SHH activity is dependent on PRMT5. We found that GLI1 isolated from SHH-MB tissues is highly methylated, including three PRMT5 sites that affect SHH-MB cell viability. Importantly, tumor growth is decreased and survival increased in mice given PRMT5 inhibitor.

Conclusions. PRMT5 is a requisite driver of SHH-MB that regulates tumor progression. A clinically relevant PRMT5 inhibitor represents a promising candidate drug for SHH-MB therapy.

Key Points

- PRMT5 is a required driver of SONIC HEDGEHOG Subgroup medulloblastoma.
- PRMT5 inhibitor treatment reduces of SONIC HEDGEHOG Subgroup medulloblastoma progression in mice.

Importance of the Study

SHH-MB patients are at high risk for lifelong disabilities resulting from standard-of-care treatment. Therefore, the development of therapies that directly target the molecular drivers of the disease would have a significant clinical impact. PRMT5 represents a promising therapeutic target in SHH-MB as it has previously been implicated in the regulation of GLI1, one of the ultimate effectors of SHH-driven transcription, in tissue culture cells. Thus, our study translated this work into a SHH-driven tumor, evaluating the potential of PRMT5 inhibition in SHH-MB using primary sphere cultures *ex vivo* and multiple mouse models *in vivo*. Furthermore, we show for the first time the *in vivo* methylation pattern of GLI1 in a SHH-driven tumor and the effects of a clinically relevant PRMT5 inhibitor on tumor growth. The translational significance of this work is considerable as it addresses one of the principal needs of SHH-MB patients, the development of targeted therapies.

Medulloblastoma (MB) is the most prevalent pediatric brain tumor, comprising approximately 20% of all cases.[1] Efforts to elucidate the molecular underpinnings of the disease have led to the identification of 4 major subgroups. This includes the Sonic Hedgehog MB (SHH-MB) subgroup, which is typified by aberrant activity of the Sonic Hedgehog (SHH) signaling pathway and represents approximately one-third of pediatric MB patients.[2–5] Despite this progress toward a deeper molecular genetic understanding of MB, relatively few targeted therapeutics have seen clinical success. This is concerning because, although overall survival rates are nearly 70%, standard-of-care therapies like craniospinal radiation, chemotherapy, and surgical resection leave patients at risk for lifelong cognitive disabilities.[6,7] Inhibitors of the SHH pathway's principal activator, SMOOTHENED (SMO), have received FDA approval for the treatment of basal cell carcinoma and acute myeloid leukemia. Two of these inhibitors, Vismodegib and Sonidegib, are currently undergoing clinical evaluation as a targeted therapeutic in multiple cohorts of SHH-MB patients.[8] However, despite significant early efficacy, frequent resistance and recurrence have been observed,[9] likely arising from mutations in SMO or downstream elements of the SHH pathway.[10] This unfortunate reality highlights the need for inhibitors of SHH signaling that act on elements of the pathway downstream of SMO capable of overcoming or preventing such recurrence.

In the absence of SHH, its transmembrane receptor complex, including PATCHED1 (PTCH1), functions to repress the activity of SMO[11] (see Figure 1). This allows for the association of the GLI family of transcription factors (GLI1, GLI2, and GLI3[12]) with the negative regulator SUFU.[13] These complexes are sequestered in the cytoplasm where they are phosphorylated and targeted for proteasomal degradation. Upon binding SHH, PTCH1 can no longer inhibit SMO, allowing SMO to localize in primary cilia, membrane-encased protrusions on the apical side of polarized cells.[14] This in turn promotes the trafficking of GLI proteins to the cilium tip where they become differentially phosphorylated, dissociate from SUFU, and ultimately translocate to the nucleus where they drive SHH-related transcription.[15] As GLI proteins are the terminal step in SHH activation, they represent the most attractive target for the treatment of SHH-MB. Despite such potential, no drugs targeting GLI transcription factors have had significant clinical impact.

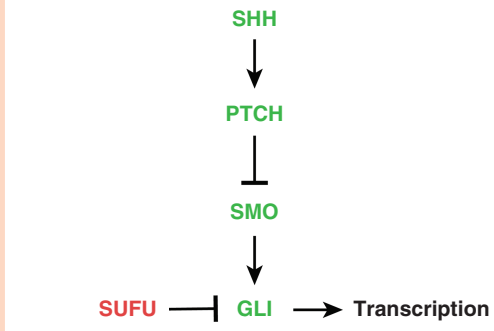

Figure 1. Schematic representation of the SHH signaling pathway. Positive regulators are depicted in green while negative regulators are shown in red.

As such, druggable proteins that indirectly regulate GLI proteins may provide an alternative method of inhibiting GLI activity in SHH-MB therapy.

Posttranslational modifications (PTMs) represent one potentially targetable regulatory mechanism of GLI proteins, as the enzymes responsible for such modifications could be exploited therapeutically. While the roles of phosphorylation,[16] ubiquitination,[17] and acetylation[18] in GLI regulation have received considerable attention, the effect of arginine methylation has only begun to be explored. Arginine methylation is a common PTM catalyzed by a family of nine enzymes known as protein arginine methyltransferases (PRMTs). PRMTs are categorized into three types based on the methylation they catalyze: Type I, which form asymmetric dimethylarginine; Type II, which produce symmetric dimethylarginine; and Type III, which catalyze monomethylarginine. The regulation of many cellular processes, including mitosis, splicing, and transcription is dependent on the activity of the PRMT family of enzymes.[19] Multiple PRMTs have also been shown to contribute to the development of human cancers, including the predominant Type II PRMT, PRMT5.[20,21] Interestingly, PRMT5 was also shown to regulate GLI1 activity in a SHH responsive tissue culture cell line.[22] Further, this group

identified a series of potential PRMT5 methylation sites on GLI1 using an *in vitro* methylation assay, a number of which were shown to be important functionally for GLI1 stability.

We speculated that PRMT5 might play a significant role in a SHH-driven cancer such as SHH-MB and now show that PRMT5 is overexpressed in SHH-MB, where it interacts with GLI1. We used both RNAi-mediated knockdown and pharmacological inhibition to demonstrate that loss of PRMT5 activity in SHH-MB sphere cultures leads to reductions in cell viability and SHH signaling. We next identified PRMT5 methylation sites on GLI1 isolated from a SHH-driven MB tissue, providing for the first time direct evidence that GLI1 is methylated *in vivo*. Importantly, we show that a clinically relevant PRMT5 inhibitor can attenuate SHH-MB progression *in vivo*. Collectively, our results suggest that PRMT5 is an important regulator of SHH-MB progression and highlights the promise of a clinically relevant PRMT5 inhibitor in late-stage clinical development to target SHH-driven cancers such as SHH-MB.

Materials and Methods

Bioinformatics

Patient datasets were downloaded as log normalized expression set matrices from the NCBI GEO with accession numbers GSE74195, GSE50161, GSE68015, GSE42656, and GSE37385. The data were then analyzed in R 4.1.2 using the GEOquery[23] and dplyr packages. No batch correction was performed and the data were not combined. Thus, each dataset is treated as a separate entity.

Cell Culture and Reagents

SMO agonist (SAG) treatments in NIH3T3 were performed in DMEM with 0.5% FBS and 100 nM SAG (SCBT). The medulloblastoma sphere cultures MSC2 (*PTCH1*$^{-/-}$*;TRP53*$^{-/-}$) and MSC4 (*PTCH1*$^{-/-}$*;TRP53*$^{+/+}$) were previously isolated in our lab[24,25] and were cultured in MSC media (DMEM/F12 media (Lonza) supplemented with HEPES, L-Glutamine, and B-27 (Thermo Fisher Scientific)) for a maximum of 10 passages. MSC4R cells were selected for vismodegib resistance by culturing them in Neurobasal media with Glutamax (1%), B-27 (2%), N-2 (1%), EGF (25 ng/mL), and FGF (25 ng/mL), all purchased from Thermo Fisher Scientific, for 5 days.[26] *SUFU*$^{-/-}$ immortalized MEFs were provided by Dr. Rune Toftgård (Karolinska Institutet) and cultured in DMEM supplemented with 10% FBS, penicillin, and streptomycin. Granular cell progenitors (GCPs) were isolated and cultured as previously described using a Papain dissociation system (Worthington).[27]

LIGHT2 SHH Activity Reporter Assay

All siRNA were purchased as Smartpools from Dharamacon. Cells were transfected with 50 nM siRNA using Lipofectamine RNAiMAX (Thermo Fisher Scientific) as per the manufacturer's instructions. After 48 hours, media was changed to DMEM with 0.5% NBCS supplemented with either 100 nM SAG or an equivalent amount of DMSO. Twenty-four hours later, cells were lysed and luminescence assayed using a dual luciferase reporter assay kit (Promega).

Antibody Based Analyses

For immunoblotting, cells were lysed in 1X Laemmli sample buffer (BioRad) or RIPA (Thermo Fisher Scientific) and boiled before SDS-PAGE. Immunoblots were visualized on autoradiography film (VWR) or a BioRad ChemiDoc MP imaging system (BioRad). Quantification of immunoblots was performed using ImageJ.[28]

For immunoprecipitation intended for downstream LC-MS/MS analysis, mouse MB tissue was homogenized and lysed for 30 minutes on ice using IP lysis buffer A (see supplementary). The lysate was then centrifuged at 2000 × g for 15 minutes and the resulting supernatant centrifuged at 16,000 × g for 30 minutes. A total of 20 µg of custom GLI1 polyclonal antibodies[29] or rabbit IgG (Jackson ImmunoResearch Laboratories) was then added to the supernatant and rotated overnight at 4°C. Protein A/G Plus agarose beads (Santa Cruz Biotechnology) were then added and rotated for 4 hours at 4°C. The beads were then centrifuged, washed twice with IP lysis buffer A containing 500 mM NaCl, and twice with normal IP lysis buffer A. The antibody bound beads were then resuspended in 50 µL Laemmli buffer, boiled, used in SDS-PAGE, and analyzed by LC–MS/MS.

For all other immunoprecipitations, cells were lysed in Thermo Fisher Scientific IP Lysis Buffer supplemented with HALT protease inhibitor cocktail. One-hundred µg of total protein was then rotated overnight at 4°C with 2 µg of GLI1 antibodies.[29] The following day, Protein A/G Plus agarose beads were added and rotated for an additional for 4 hours. Antibody-bound beads were then washed 3 times with 25 mM Tris–HCl (pH 7.4), 300 mM NaCl, 1 mM EDTA, 1% NP-40, and 5% glycerol before resuspension in Laemmli buffer, boiling, and immunoblotting.

LC–MS/MS

Gel bands were excised, reduced with TCEP, alkylated with iodoacetamide, and digested in-gel with trypsin. LC–MS/MS was performed using a Q Exactive HF mass spectrometer (Thermo Fisher Scientific) coupled with a Nano-ACQUITY UPLC system (Waters). Samples were injected onto a UPLC Symmetry trap column (180 µm i.d. × 2 cm packed with 5 µm C18 resin; Waters). Tryptic peptides were separated by reversed-phase HPLC on a BEH C18 nanocapillary analytical column (75 µm i.d. × 25 cm, 1.7 µm particle size; Waters) using a 90 min gradient formed by solvent A (0.1% formic acid in water) and solvent B (0.1% formic acid in acetonitrile). Eluted peptides were analyzed by the mass spectrometer set to repetitively scan m/z from 400 to 2000 in positive ion mode. The full MS scan was collected at 60,000 resolution followed by data-dependent MS/MS scans at 15,000 resolution on the 20 most abundant ions exceeding a minimum threshold

of 10,000. Peptide match was set as preferred, exclude isotopes option and charge-state screening were enabled to reject singly and unassigned charged ions. Peptide sequences and methyl-arginylation sites were identified using MaxQuant 1.6.1.0.[30] MS/MS spectra were searched against a UniProt mouse protein database (10/01/2017) using full tryptic specificity with up to two missed cleavages, static carboxamidomethylation of Cys, and variable Met oxidation, Arg methylation (mono, di, tri), and protein N-terminal acetylation. Consensus identification lists were generated with false discovery rates of 1% at protein, peptide, and site levels.

Lentiviral Transductions

Lentiviral shRNA plasmids in the pLKO.1 vector were purchased from Horizon Discovery. Lentivirus was produced by cotransfecting HEK293T with lentivirus plasmid and packaging plasmids pAX2 and pMDG.2 with Lipofectamine 2000 (Thermo Fisher Scientific) in OptiMEM media (Thermo Fisher Scientific). Transfected cells were then cultured for 72 hours before media was filtered using a sterile 0.45 μm syringe filter. Filtered media was mixed with Lenti-X Concentrator solution (Takara) and centrifuged as per the manufacturer's recommendations. The resulting pellet was resuspended in MSC media and titered using the QuickTiter Lentivirus Titer Kit (Cell Biolabs, Inc.).

SHH-MB sphere cultures were dissociated using Accutase Cell Dissociation Reagent (Thermo Fisher Scientific) before filtration through a 70 μm cell strainer (Corning), centrifugation at 200 × g, and resuspension in MSC media at 1×10^6 cells/mL. Lentivirus was then added at an MOI of 10, along with 8 μg/mL polybrene (Sigma Aldrich). This mixture was then centrifuged at 200 × g for 2 hours. Cells were kept in culture after transduction for 4 days when determining mRNA expression or 6 days before evaluating cell viability via a MTT reduction assay.[24]

RNA Expression

Total RNA was extracted using the RNAeasy Plus RNA Extraction Kit (Qiagen). RNA was then quantified using a NanoDrop spectrophotometer (Thermo Fisher Scientific) and cDNA produced using the High-Capacity RNA to cDNA Kit (Thermo Fisher Scientific). Gene expression was then determined using Universal qPCR Mastermix (Thermo Fisher Scientific) with Taqman Gene Expression Assays (Thermo Fisher Scientific) on a BioRad CFX96 qPCR thermocycler. Data are normalized to mouse *β ACTIN* (*ACTB)* expression.

Ex vivo Drug Treatment

GSK3326595 treatments studying SHH-MB sphere culture cell viability were conducted for 10 days (changing media/drug every 3 days) and those evaluating biomarkers were conducted for 4 days. Vismodegib treatments were conducted for 72 hours. Cell viability was determined via an MTT reduction assay. Studies using GSK3326595 in *SUFU*$^{-/-}$ immortalized MEFs and GCPs were also carried out over 4 days.

Ectopic Expression of GLI1 Mutants

Plasmid DNA was electroporated into MSC4 cells using the P3 Primary Cell 4D X Kit and a Nucleoporator (Lonza). After 96 hours, cell viability was measured using the Cell-Titer Glo Kit (Promega).

In Vivo Procedures

All mouse work was conducted in accordance with University of Miami IACUC protocol #19-095adm4. *ND2:SMOA1* mice (Jackson Laboratory strain 008831) have been genetically modified such that an SMO mutant transgene that is constitutively active is expressed from the *NEUROD2* promoter,[31] restricting its expression to the cerebellum. To generate the primary tissue used in LC-MS/MS analysis, CD-1 Nude mouse (Charles Rivers Laboratories stock 086) flanks were implanted with primary murine SHH-MB tissue. Orthotopic implantations were performed as previously described.[24] MSC4 cells were transduced with CMV-Firefly luciferase lentivirus (Cellomics). These cells were grown for several days and frozen for later use. After reviving them, spheres were treated with Accutase and 3 μL was implanted at a concentration of 1.0×10^5 cells/mL in DMEM/F12 2 mm posterior to the lambda suture, 2 mm lateral of the sagittal suture, and 2 mm deep in CD-1 Nude mice. Cells were injected over a period of 1 minute and the needle was held in place for an additional minute following injection. One-hundred mM GSK3326595 stocks in DMSO were diluted in 0.5% methylcellulose (Sigma Aldrich) such that the final concentration allowed for the administration of 200 mg/kg in 100 μL via oral gavage every day. Vehicle controls were treated with equal volumes of the DMSO/methylcellulose mixture. Luminescence was imaged using a Perkin Elmer IVIS Spectrum 10 minutes following the intraperitoneal injection of D-Luciferin (Perkin Elmer). For immunoblotting of tumor tissue, orthotopic allografts were implanted before treatment as above. When mice displayed symptoms of SHH-MB, they were euthanized and tumor tissue isolated, homogenized, and lysed in RIPA buffer with HALT protease inhibitors before immunoblotting. To assess mouse survival with PRMT5 inhibition, *ND2:SMOA1* litters were allowed to reach 2 months of age before GSK3326595 or vehicle was administered using the same schedule and dosage as above for 30 days.

Statistical Analysis

In vivo tumor volume studies are shown as the mean and SEM of 4 mice for each group normalized to the luminescence intensity seen in each mouse at the first reading. Survival was assessed using a Kaplan-Meier survival analysis with 18 mice in each group and significance determined using a Log Rank Mantel-Cox test. Significance was defined as $P < .05$ and indicated via an asterisk. Plots were produced in GraphPad Prism 9.

Results

PRMT5 is Overexpressed in SHH-MB

We first examined the expression of PRMT5 in SHH-MB tissue relative to normal cerebellum. We found that *PRMT5* is more highly expressed in MB relative to normal cerebellar tissue in four distinct cohorts of MB patients (Figure 2A).[32–35] Similarly, resected MB tissue from SHH-MB patients expressed higher levels of *PRMT5* compared to MB patients of other subgroups (Figure 2B).[36] PRMT5 protein levels were also increased in granular cell progenitors (GCPs), the putative cell of origin of SHH-MB isolated from *ND2:SMOA1* mice compared to those isolated from wildtype mice (Figure 2C and D). *ND2:SMOA1* mice are a GEMM that spontaneously develops SHH-MB tumors due to an activating mutation in a transgenic SMO.[31] Similarly, PRMT5 protein levels were elevated in *ND2:SMOA1* MB tissue, relative to normal cerebellum, when analyzed by immunoblotting (Figure 2E and F). Global symmetric dimethylarginine (SDMA), a biomarker for PRMT5 activity, is also elevated in tumor tissue compared to normal cerebellum controls. These results show that PRMT5 and a surrogate for PRMT5 activity are elevated in SHH-MB tumors.

PRMT5 is Required for SHH-MB Cell Viability

We evaluated the role of PRMT5 in SHH-signaling using a commonly used SHH reporter cell line, LIGHT2. We attenuated *PRMT5* expression in LIGHT2 cells using siRNA and found that SHH-activity is decreased upon *PRMT5* knockdown (Figure 3A). We also noted that PRMT5 levels

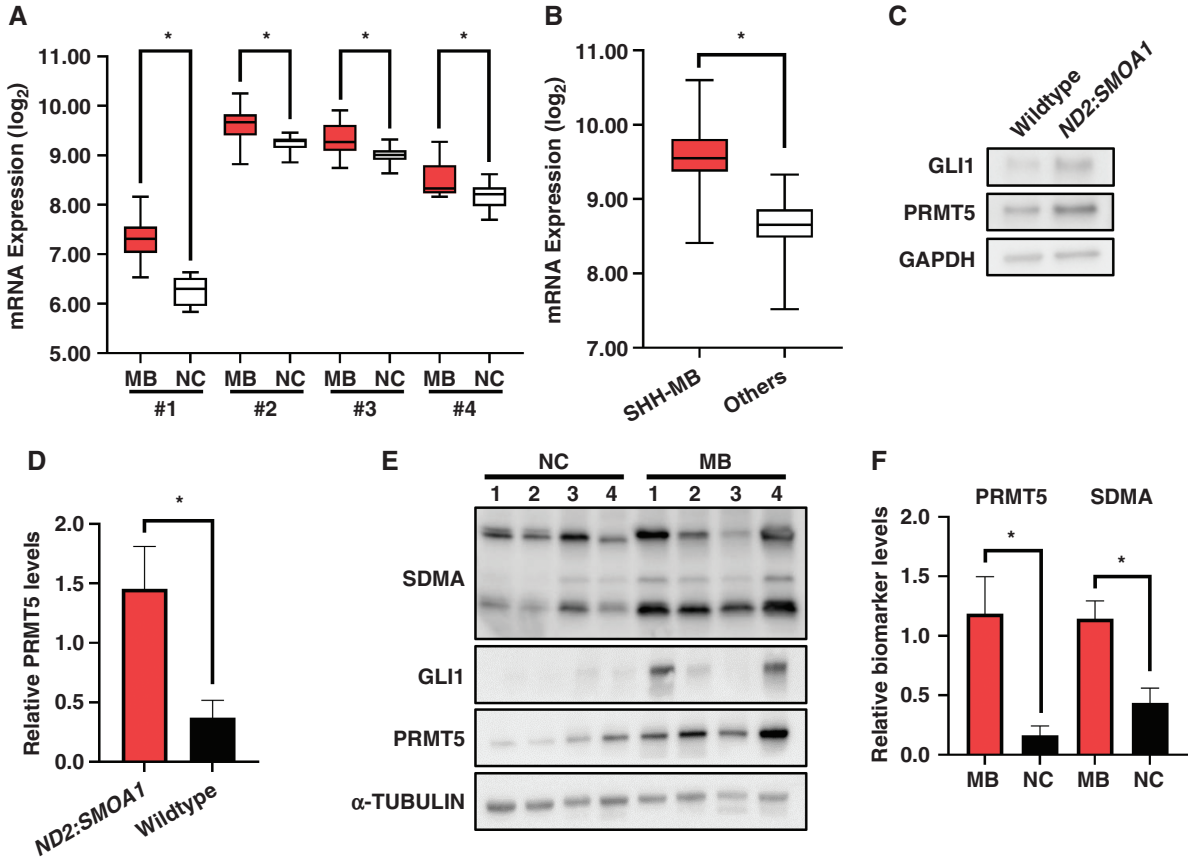

Figure 2. PRMT5 is overexpressed in SHH-MB. A) Comparison of *PRMT5* RNA levels in patient derived SHH-MB tissue (labeled as MB) with control cerebellum (labelled as NC), using data from 4 separate studies[32–35] without batch correction or normalization. Significance was determined using a *t*-test ($P < .05$) and is indicated with asterisks. B) Comparison of *PRMT5* RNA levels in patient derived SHH-MB tissue with tissue from other subgroups of MB patients.[36] Significance was determined using a *t*-test ($P < .05$) and is indicated with asterisks. C) Granular cell progenitors were isolated from either wildtype or *ND2:SMOA1* mice. After culturing in media supplemented with 100 nM SAG for 24 hours, cells were lysed in RIPA buffer and immunoblotted for the indicated proteins. A representative blot from 1 of 3 biological replicates is shown. D) Quantitation of immunoblotting for the PRMT5 protein levels normalized to GAPDH. Data represent the mean and SEM of 3 biological replicates. Significance was determined using a *t*-test ($P < .05$) and is indicated with asterisks. E) MB and cerebellar tissue (labelled as NC) taken from 4 separate symptomatic *ND2:SMOA1* mice were lysed in RIPA buffer and analyzed by immunoblotting to determine the levels of the indicated proteins. F) Quantitation of proteins from the immunoblot shown in E normalized to α-TUBULIN. Significance was determined using a *t*-test ($P < .05$) and is indicated with asterisks.

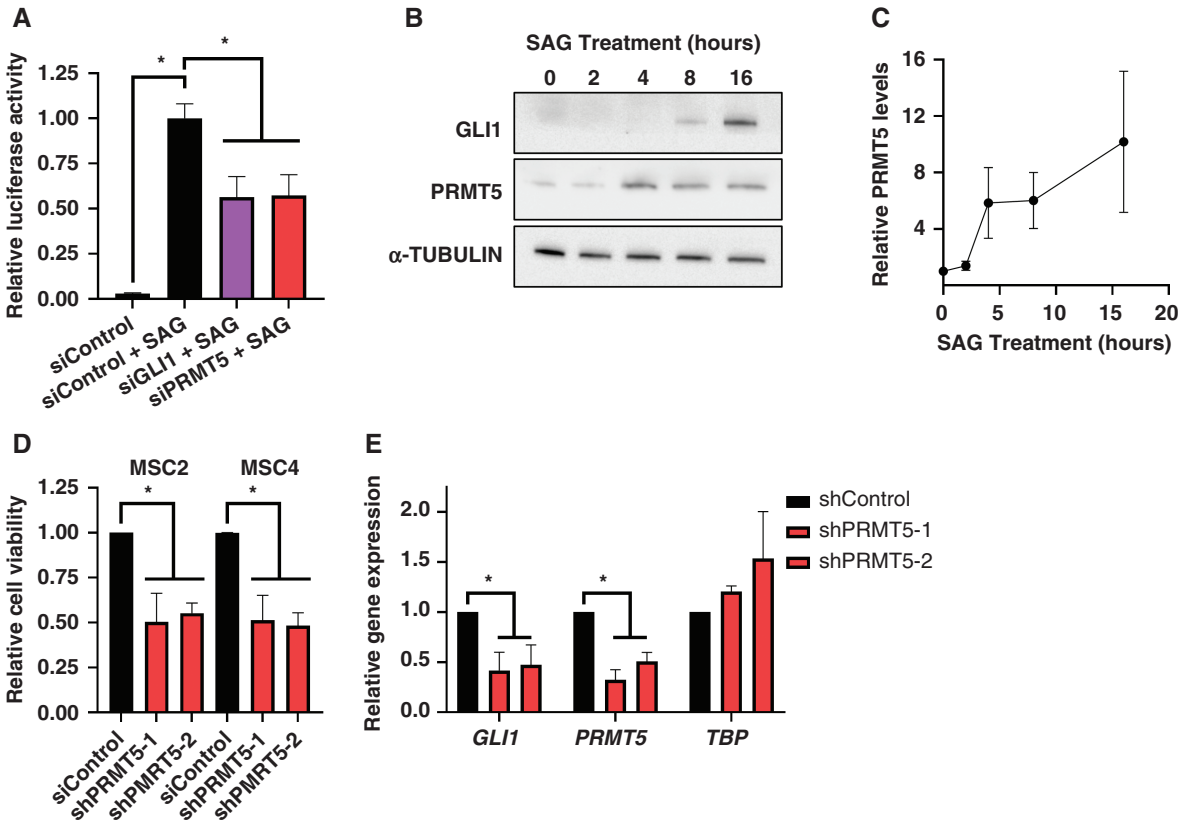

Figure 3. PRMT5 is required for SHH-MB cell viability. A) LIGHT2 cells were treated with the indicated siRNA for 48 hours before the addition of 100 nM SAG or a DMSO control for an additional 24 hours. Data are normalized to the SAG-treated siRNA control and represent the mean and SEM of 3 biological replicates. Significance was determined using a *t*-test ($P < .05$) and is indicated with asterisks. B) NIH3T3 were treated with 100 nM SAG for the indicated times before lysing in RIPA buffer and immunoblotting for the indicated proteins. A representative immunoblot of 3 biological replicates is shown. C) Quantitation of immunoblotting for PRMT5 protein levels in samples described in B. Data are normalized to α-TUBULIN and then the 0-hour sample and represent the mean and SEM of 3 biological replicates. D) SHH-MB sphere cultures were transduced with lentivirus bearing either a nontargeting shRNA control or shRNA targeting *PRMT5* for 6 days, followed by evaluation of cell viability via an MTT reduction assay. Data are normalized to the nontargeting control and represent the mean and SEM of 3 biological replicates. Significance was determined using a t-test ($P < .05$) and is indicated with asterisks. E) RNA was collected from SHH-MB sphere cultures treated with lentivirus containing a non-targeting control or shRNA against *PRMT5* for a period of 4 days. This RNA was then analyzed by RT-qPCR to determine the expression level of the indicated genes. Data are normalized to the control shRNA-treated sample and represent the mean and SEM of 3 biological replicates. Significance was determined using a *t*-test ($P < .05$) and is indicated with asterisks.

were increased in response to SHH activity induced by the small molecule SMO agonist SAG in NIH3T3 cells (Figure 3B and C). To determine if PRMT5 is required for MB cell growth, we used 2 separate SHH-MB sphere cultures that were previously isolated from a primary murine SHH-MB tumor.[24,25] These cells posses constitutive SHH activity due to loss of *PTCH1* function. They also have distinct genetic backgrounds, one harboring *TP53* mutations (MSC2) and one with wild-type *TP53* (MSC4). We used these cultures because they retain their dependence on SHH signaling in culture,[24,25] unlike immortalized SHH-MB cell lines.[37] We knocked down the expression of *PRMT5* in these SHH-MB sphere cultures and measured cell viability or the expression of an SHH target gene, relative to a nontargeting shRNA control. A reduction of both cell viability (Figure 3D) and the expression of *GLI1* (Figure 3E) was observed upon *PRMT5* knockdown, relative to the expression of the housekeeping gene *TBP*. This observation distinguishes PRMT5's role in SHH-MB from that of a number of other cancers, where it has been shown that the efficacy of PRMT5 inhibitors is correlated with *TP53* status.[38,39]

A Clinically Relevant PRMT5 Inhibitor Attenuates SHH-MB Cell Viability

A number of selective PRMT5 inhibitors have been developed, some of which are undergoing clinical evaluation. This includes GSK3326595 (also known as Pemrametostat or EPZ015938), which is currently in Phase II clinical trials for breast cancer (clinicaltrials.gov identifier NCT04676516). To validate the effect of GSK3326595 on SHH activity, we treated *SUFU*$^{-/-}$immortalized MEFs that have constitutive SHH activity with the drug. GSK3326595 reduced the

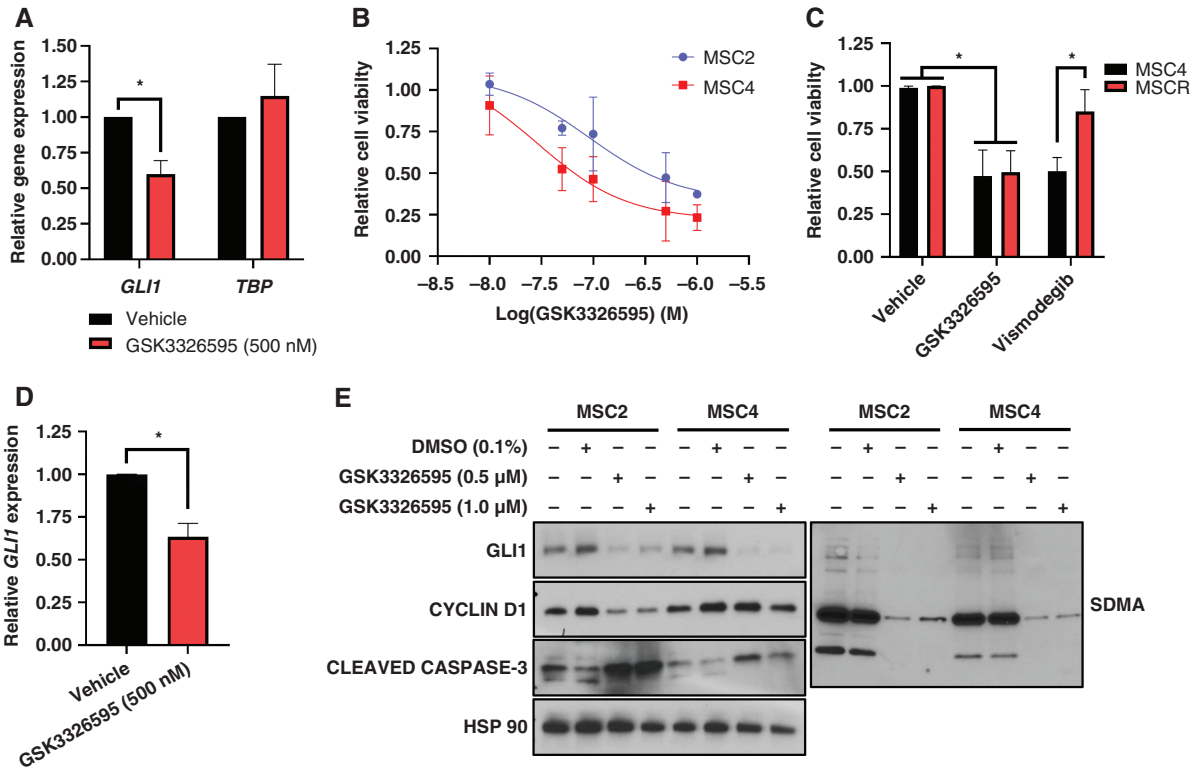

Figure 4. A clinically relevant PRMT5 inhibitor attenuates SHH-MB cell viability. A) *SUFU*$^{-/-}$ immortalized MEFs were treated with the indicated concentration of GSK3326595 for 96 hours prior to RNA extraction and analysis by RT-qPCR for the indicated genes. Data are normalized to the vehicle control and represent the mean and SEM of 3 biological replicates. Significance was determined using a *t*-test ($P < .05$) and is indicated with asterisks. B) SHH-MB sphere cultures were treated with the indicated concentrations of GSK3326595 for a period of 10 days prior to the evaluation of cell viability via a MTT reduction assay. Data are normalized to the vehicle control and represent the mean and SEM of 3 biological replicates. C) Vismodegib resistant MSC4 cells (MSC4R) were treated with 100 nM GSK3326595 for a period of 10 days or 2 µM vismodegib for 72 hours prior to determining cell viability via a MTT reduction assay. Data represent the mean and SEM of 3 biological replicates. Significance was determined using a *t*-test ($P < .05$) and is indicated with asterisks. D) RNA was collected from SHH-MB sphere cultures treated with either vehicle or GSK3326595 and analyzed by RT-qPCR for the expression of the SHH target gene *GLI1* relative to *ACTB*. Data are normalized to the vehicle control and represent the mean and SEM of 3 biological replicates. Significance was determined using a *t*-test ($P < .05$) and is indicated with asterisks. E) SHH-MB sphere cultures were treated with the indicated concentrations of GSK3326595 or vehicle control for 96 hours prior to lysis and immunoblotting for the indicated proteins. A representative immunoblot of 3 biological replicates is shown.

expression of *GLI1* in *SUFU*$^{-/-}$immortalized MEFs (Figure 4A), consistent with it attenuating SHH activity and doing so acting downstream of SMO. Notably, SHH signaling is resistant to vismodegib in these cells.[24] We next examined the impact of PRMT5 activity on the tumorigenic properties of SHH-MB by treating 2 distinct SHH-MB sphere cultures with GSK3326595. The viability of these cultures was reduced in a dose-dependent manner, with an approximate IC_{50} of 300 and 80 nM in MSC2 and MSC4 respectively (Figure 4B). GSK3326595 has a similar IC_{50} in MSC4 cells selected for resistance to vismodegib,[26] designated MSC4R (Figure 4C). Reduction in the expression of the SHH target gene *GLI1* is also seen in MSC4 upon PRMT5 inhibitor treatment (Figure 4D), as were GLI1 protein levels (Figure 4E). A decrease in both CYCLIN-D1, a biomarker of SHH activity and cell proliferation, and SDMA, a biomarker for PRMT5 activity, was also observed (Figure 4E). An increase in the level of the apoptotic biomarker cleaved CASPASE-3 was also seen in response to PRMT5 inhibitor treatment (Figure 4E). In sum, these results reveal that PRMT5 activity is essential for cell viability and GLI activity in SHH-MB sphere cultures, likely through attenuation of proliferation and increased apoptosis.

GLI1 is Methylated in SHH-MB Tissue

We reasoned that, if PRMT5 regulation is an important driver of SHH activity, GLI1 should be highly methylated in SHH-MB. We therefore immunopurified endogenous GLI1 from MB tissue isolated from a SHH-MB mouse model and analyzed these samples by LC–MS/MS to identify methylated GLI1 residues. This approach yielded 13 methylated arginines that are conserved in human GLI1 (Figure 5A). Three of these residues (R517, R599, and R995) were dimethylated, making these arginines potential PRMT5 substrates. These residues are conserved in human GLI1 as R515, R597, and R990 (Figure 5B) and were

A

Mouse GLI1 arginine methylation sites	Conserved human sites
R103	R100
R241	R238
R280	R277
R512	R510
R517	R515
R599	R597
R623	R621
R639	R637
R806	R805
R985	R980
R989	R984
R995	R990
R1023	R1018

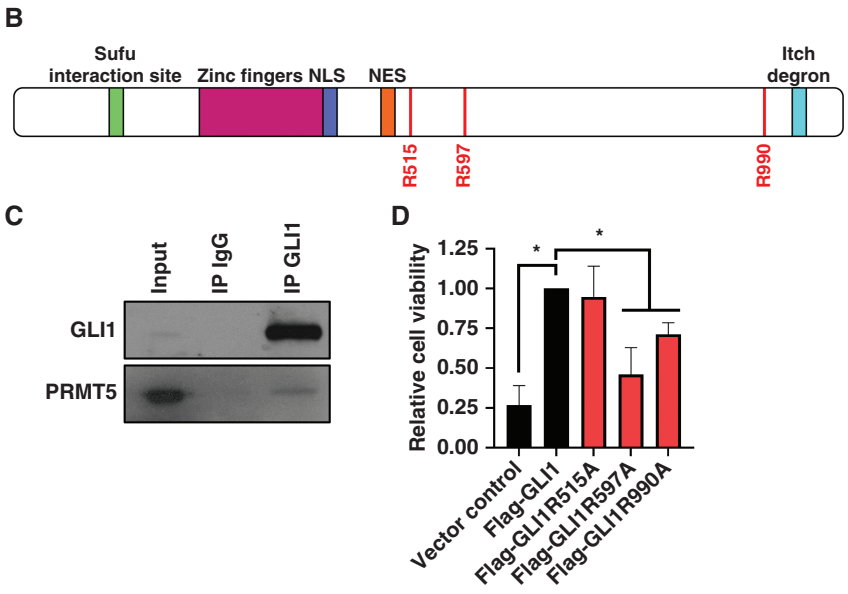

Figure 5. GLI1 is methylated on PRMT5 sites in SHH-MB tissue. GLI1 was immunopurified from an SHH-MB tumor grown in the flank of a CD-1 Nude mouse. The arginine methylation status of GLI1 was then determined using LC/MS-MS. A) Table showing the methylated arginines identified in murine GLI1 by LC-MS/MS and the conserved residues in human GLI1. Red shading indicates dimethylated putative PRMT5 sites, as previously described.[19] B) A schematic of GLI1 with key motifs highlighted. The putative PRMT5 substrate sites conserved in human GLI1 are highlighted in red. C) GLI1 was immunoprecipitated (IP GLI1) relative to a control immunoprecipitation (IP IgG) from SHH-MB sphere cultures and immunoblots performed for the indicated proteins. D) MSC4 cells were electroporated with the indicated plasmids and cell viability measured 96 hours later using a Cell-Titer Glo assay. Data are normalized to Flag-GLI1 and represent the mean and SEM of 3 biological replicates. Significance was determined using a *t*-test ($P < .05$) and is indicated with asterisks.

previously shown to be directly methylated by PRMT5 in an *in vitro* biochemical assay.[22] Also, consistent with PRMT5 directly methylating GLI1 in SHH-MB, PRMT5 and GLI1 co-immunoprecipitate from primary SHH-MB tissue (Figure 5C). Furthermore, the viability of MSC4 cells ectopically expressing loss-of-function mutations at R597 or R990 is significantly reduced relative to wildtype GLI1, suggesting they play a functionally significant role in SHH-MB (Figure 5D).

PRMT5 is Required for SHH-MB Progression *In Vivo*

Based on our *ex vivo* experiments, we hypothesized that PRMT5 is required for MB progression. We therefore treated GCPs isolated from a genetically engineered mouse MB model, *ND2:SMOA1*,[31] with either GSK3326595 or a vehicle control. Such cells showed reduced GLI1 levels as well as lower levels of PCNA, a biomarker for cell proliferation when treated with GSK3326595 (Figure 6A). *ND2:SMOA1* mice were also given daily oral administration of GSK3326595 over a 30-day period, and this treatment resulted in significantly increased survival relative to control mice (Figure 6B). Importantly, the SMO variant expressed in *ND2:SMOA1* mice harbors a mutation that renders them resistant to vismodegib.[31,40,41] An orthotopic *PTCH1* driven SHH-MB mouse model was also treated daily with this PRMT5 inhibitor and the average volume of tumors determined by IVIS imaging. Tumors in mice treated with PRMT5 inhibitor were reduced in size relative to the vehicle control (Figure 6C). The average reduction in luminescence intensity for this cohort of mice over the course of the experiment, is also shown in Figure 6D. SDMA is also significantly reduced in tumor tissue isolated from similarly treated mice, demonstrating the effect of GSK3326595 on PRMT5 activity (Figure 6E and F). Together, these results provide evidence that PRMT5 inhibition reduces SHH-MB progression *in vivo*.

Discussion

Here, we evaluate the functional significance of PRMT5 and the potential of a clinically relevant PRMT5 inhibitor in SHH-MB. We found that PRMT5 is overexpressed in SHH-MB tissue and that GLI1 originating from such primary SHH-MB tissue is methylated at a number of PRMT5 consensus sites, some of which are important for SHH-MB cell viability. We also found that GLI1 associates with PRMT5 in this tissue. Furthermore, shRNA-mediated knockdown and pharmacological inhibition revealed that PRMT5 regulates SHH-MB cell viability and SHH activity in such cells. Most importantly, we were able to attenuate SHH-MB progression in two distinct mouse MB models using a clinically relevant PRMT5 inhibitor. Thus, our work suggests that PRMT5 is an important regulator of SHH-MB,

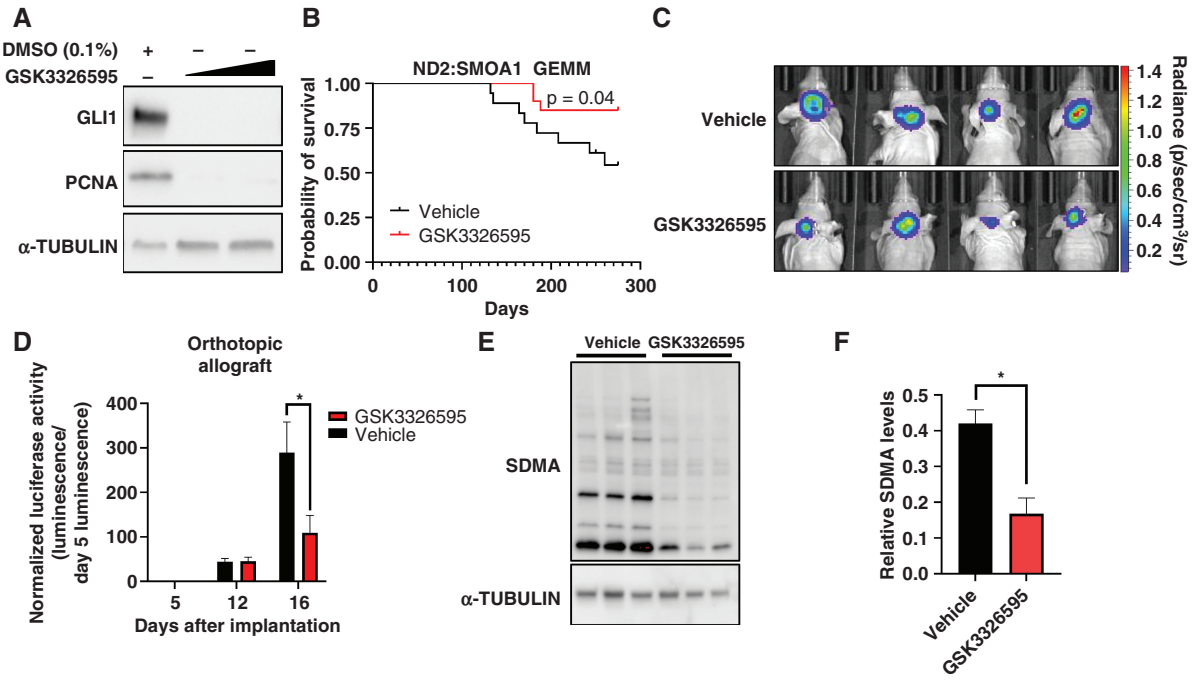

Figure 6. PRMT5 is required for SHH-MB progression *in vivo*. A) GCPs isolated from *ND2:SMOA1* mice were treated with either a vehicle control or GSK3326595 (0.5 or 1 μM) for 4 days prior to lysis in RIPA buffer and immunoblotting for the indicated proteins. B) *ND2:SMOA1* mice were treated with either GSK3326595 (shown in red) or a vehicle control (shown in black) every day for a period of 30 days. Symptom free survival curves are shown and significance was determined using a Log Rank test. C) SHH-MB sphere cultures constitutively expressing luciferase were implanted into the cerebella of CD-1 nude mice. Animals were then treated with a clinically relevant PRMT5 inhibitor (GSK3326595) or vehicle and the tumors visualized using IVIS. A representative image of 4 mice from each treatment group shown at day 16. D) Quantification of the luminescence signal of each mouse was measured and the average and SEM plotted. The luminescence activity of each individual mouse is normalized to the luminescence activity of the same mouse in the first IVIS imaging at day 5 with the vehicle treated group depicted in black and the PRMT5 inhibitor treated group in red. A *t*-test was used to determine statistical significance ($P < .05$) and is indicated with an asterisk. E) Mice with orthotopic SHH-MB allografts were treated with either vehicle or GSK3326595. When mice displayed symptoms of SHH-MB, mice were euthanized and tumor tissue isolated. Tissue was then lysed in RIPA buffer and immunoblotted. F) Quantitation of immunoblotting for SDMA in samples shown in E. Data are normalized to α-TUBULIN and represent the mean and SEM of 3 biological replicates. Significance was determined using a *t*-test ($P < .05$) and is indicated with asterisks.

which could serve as an important, druggable regulator of GLI activity in SHH-driven cancers such as SHH-MB.

As GLI1 methylation was implicated in GLI1 regulation in the SHH responsive mesenchymal cell line C3H10T1/2, we hypothesized that GLI1 would be methylated in SHH-dependent tumors like SHH-MB. This analysis revealed that a subset of these methylated arginines were dimethylated, accordant with them being methylated by a Type II PRMT such as PRMT5. This is the first direct identification of arginine methylation sites in GLI1 from primary SHH-driven tumor tissue. Furthermore, we found that PRMT5 associated with GLI1, which is consistent with GLI1 being a direct substrate of PRMT5. Importantly, 4 of the conserved arginines in human GLI1, arginines 515, 597, 990, and 1018, have been previously shown to play a functional role in the stability of GLI1 in C3H10T1/2 cells (Figure 5A).[22] A subset of these residues was found to be crucial in SHH-MB sphere culture viability (Figure 5D). We suggest that PRMT5 enhances the tumorigenic properties of SHH-MB via this increase in GLI1 stability. This model is consistent with the reduction in GLI1 protein levels we observed upon PRMT5 inhibition (Figure 4E).

Importantly, the clinically relevant drug used in this study, GSK3326595, is a substrate competitive selective PRMT5 inhibitor currently in phase II clinical trials for use in early-stage breast cancer. Since medulloblastoma is a relatively rare disease, drugs in development for its treatment may be granted Orphan designation by the FDA. Repurposed inhibitors are therefore particularly attractive as they can be transitioned into the clinic more feasibly and rapidly. Our findings suggest that GSK3326595 is an attractive candidate therapeutic for such a repurposing in SHH-MB. This may be especially true since its inhibition of SHH activity occurs downstream of SMO and is effective in vismodegib-resistant models *ex vivo* and *in vivo*, which may allow the drug to overcome or prevent the resistance to SMO inhibitors commonly observed in SHH-MB patients.

In conclusion, our findings demonstrate that PRMT5 is a key regulator of SHH-MB tumorigenicity. Furthermore, we show that the use of a clinically relevant PRMT5 inhibitor reduces SHH-MB progression *in vivo*. Taken together, our findings provide compelling evidence supporting the development of PRMT5 inhibitors for the treatment of SHH-MB.

Supplementary Material

Supplementary material is available at *Neuro-Oncology Advances* online.

Keywords

cancer | GLI | medulloblastoma | PRMT5 | SHH

Acknowledgments

We thank all members of the Robbins lab for their comments and advice throughout the preparation of this manuscript. We thank Sylvester Cancer Center Cancer Modeling Shared Resource for providing IVIS imaging, the Department of Surgery Tissue and Pathology core for assistance in tumor sample processing, and the Wistar Institute Proteomics Facility for performing LC–MS/MS analysis.

Funding

National Institutes of Health (R01NS110591 to D.J.R., R50CA221838 to H.Y.T); National Cancer Institute (T32 CA009686 to D.T.W.); FDOH, Live Like Bella Pediatric Cancer Research Initiative (8LA03 to D.J.R.); American Cancer Society Institutional Research Grant awarded to the Hollings Cancer Center: IRG-19-137-20 (J.R.B.); Rally Foundation Career Development Award: 20CDN46 (J.R.B.); National Institute of Neurological Disorders and Stroke of the National Institutes of Health Award: K01NS119351 (J.R.B), SCTR grant UL1TR001450 (J.R.B).

Conflict of interest statement: The authors declare no conflicts of interest.

Author contributions

Experimental Design: D.T.W, J.R.B., J.L, H.Y.T., D.J.R. Experimental Execution: D.T.W, J.R.B., J.L., F.Y., D.F., C.S., H.Y.T. Data Analysis: D.T.W, J.R.B., H.Y.T., D.J.R. Clinical Insight: D.H. Manuscript writing: D.T.W., D.J.R.

References

1. Louis DN, Perry A, Reifenberger G, et al. The 2016 World Health Organization classification of tumors of the central nervous system: a summary. *Acta Neuropathol.* 2016;131(6):803–820.
2. Northcott PA, Buchhalter I, Morrissy AS, et al. The whole-genome landscape of medulloblastoma subtypes. *Nature.* 2017;547(7663):311–317.
3. Parsons DW, Li M, Zhang X, et al. The genetic landscape of the childhood cancer medulloblastoma. *Science (New York, NY).* 2011;331(6016):435–439.
4. Taylor MD, Northcott PA, Korshunov A, et al. Molecular subgroups of medulloblastoma: the current consensus. *Acta Neuropathol.* 2012;123(4):465–472.
5. Louis DN, Perry A, Burger P, et al. International society of neuropathology--Haarlem consensus guidelines for nervous system tumor classification and grading. *Brain Pathol.* 2014;24(5):429–435.
6. Packer RJ, Cogen P, Vezina G, Rorke LB. Medulloblastoma: clinical and biologic aspects. *Neuro-oncology.* 1999;1(3):232–250.
7. MacDonald TJ, Rood BR, Santi MR, et al. Advances in the diagnosis, molecular genetics, and treatment of pediatric embryonal CNS tumors. *Oncologist.* 2003;8(2):174–186.
8. Li Y, Song Q, Day BW. Phase I and phase II sonidegib and vismodegib clinical trials for the treatment of paediatric and adult MB patients: a systemic review and meta-analysis. *Acta Neuropathol Commun.* 2019;7(1):123–123.
9. Rudin CM, Hann CL, Laterra J, et al. Treatment of medulloblastoma with hedgehog pathway inhibitor GDC-0449. *N Engl J Med.* 2009;361(12):1173–1178.
10. Robinson GW, Orr BA, Wu G, et al. Vismodegib exerts targeted efficacy against recurrent sonic Hedgehog-Subgroup Medulloblastoma: results from Phase II pediatric brain tumor consortium studies PBTC-025B and PBTC-032. *J Clin Oncol.* 2015;33(24):2646–2654.
11. Ogden SK, Ascano M, Jr, Stegman MA, Robbins DJ. Regulation of Hedgehog signaling: a complex story. *Biochem Pharmacol.* 2004;67(5):805–814.
12. Ruiz i Altaba A, Mas C, Stecca B. The Gli code: an information nexus regulating cell fate, stemness and cancer. *Trends Cell Biol.* 2007;17(9):438–447.
13. Han Y, Shi Q, Jiang J. Multisite interaction with Sufu regulates Ci/Gli activity through distinct mechanisms in Hh signal transduction. *Proc Natl Acad Sci USA.* 2015;112(20):6383–6388.
14. Robbins DJ, Fei DL, Riobo NA. The Hedgehog signal transduction network. *Sci Signal.* 2012;5(246):re6.
15. Hui CC, Angers S. Gli proteins in development and disease. *Annu Rev Cell Dev Biol.* 2011;27:513–537.
16. Zhou M, Jiang J. Gli Phosphorylation Code in Hedgehog Signal Transduction. *Front Cell Dev Biol.* 2022;10:846927.
17. Zhang Q, Jiang JA-OX. Regulation of Hedgehog signal transduction by ubiquitination and deubiquitination. *Int J Mol Sci.* 2021;22(24):13338.
18. Canettieri G, Di Marcotullio L, Greco A, Coni S, et al. Histone deacetylase and Cullin3-REN(KCTD11) ubiquitin ligase interplay regulates Hedgehog signalling through Gli acetylation. *Nat Cell Biol.* 2010;12(2):132–142.
19. Blanc RS, Richard S. Arginine methylation: the coming of age. *Mol Cell.* 2017;65(1):8–24.
20. Yang Y, Bedford MT. Protein arginine methyltransferases and cancer. *Nat Rev Cancer.* 2012;13:37–50.
21. Smith E, Zhou W, Shindiapina P, et al. Recent advances in targeting protein arginine methyltransferase enzymes in cancer therapy. *Expert Opin Ther Targets.* 2018;22(6):527–545.
22. Abe Y, Suzuki Y, Kawamura K, Tanaka N. MEP50/PRMT5-mediated methylation activates GLI1 in Hedgehog signalling through inhibition of ubiquitination by the ITCH/NUMB complex. *Commun Biol.* 2019;2:23.
23. Davis S, Meltzer PS. GEOquery: a bridge between the gene expression omnibus (GEO) and BioConductor. *Bioinformatics.* 2007;23(14):1846–1847.

24. Rodriguez-Blanco J, Li B, Long J, et al. A CK1alpha activator penetrates the brain and shows efficacy against drug-resistant metastatic Medulloblastoma. *Clin Cancer Res.* 2019;25(4):1379–1388.
25. Zhao X, Ponomaryov T, Ornell KJ, et al. RAS/MAPK activation drives resistance to smo inhibition, metastasis, and tumor evolution in shh pathway-dependent tumors. *Cancer Res.* 2015;75(17):3623–3635.
26. Rodriguez-Blanco J, Pednekar L, Penas C, et al. Inhibition of WNT signaling attenuates self-renewal of SHH-subgroup medulloblastoma. *Oncogene.* 2017;36(45):6306–6314.
27. Lee HY, Greene LF, Mason CA, Manzini MC. Isolation and culture of postnatal mouse cerebellar granule neuron progenitor cells and neurons. *J Vis Exp.* 2009;(23):990
28. Schneider CA, Rasband WS, Eliceiri KW. NIH Image to ImageJ: 25 years of image analysis. *Nat Methods.* 2012;9(7):671–675.
29. Fei DL, Sanchez-Mejias A, Wang Z, et al. Hedgehog signaling regulates bladder cancer growth and tumorigenicity. *Cancer Res.* 2012;72(17):4449–4458.
30. Cox J, Mann M. MaxQuant enables high peptide identification rates, individualized p.p.b.-range mass accuracies and proteome-wide protein quantification. *Nat Biotechnol.* 2008;26(12):1367–1372.
31. Hatton BA, Villavicencio EH, Tsuchiya KD, Pritchard JI, et al. The Smo/Smo model: hedgehog-induced medulloblastoma with 90% incidence and leptomeningeal spread. *Cancer Res.* 2008;68(6):1768–1776.
32. de Bont JM, Kros JM, Passier MMCJ, Reddingius RE, et al. Differential expression and prognostic significance of SOX genes in pediatric medulloblastoma and ependymoma identified by microarray analysis. *Neuro Oncol.* 2008;10(5):648–660.
33. Griesinger AM, Birks DK, Donson AM, Amani V, et al. Characterization of distinct immunophenotypes across pediatric brain tumor types. *J Immunol.* 2013;191(9):4880–4888.
34. Gump JM, Donson AM, Birks DK, et al. Identification of targets for rational pharmacological therapy in childhood craniopharyngioma. *Acta Neuropathol Commun.* 2015;3:30.
35. Henriquez NV, Forshew T, Tatevossian R, Ellis M, et al. Comparative expression analysis reveals lineage relationships between human and murine gliomas and a dominance of glial signatures during tumor propagation in vitro. *Cancer Res.* 2013;73(18):5834–5844.
36. Northcott PA, Shih DJ, Peacock J, et al. Subgroup-specific structural variation across 1,000 medulloblastoma genomes. *Nature.* 2012;488(7409):49–56.
37. Sasai K, Romer JT, Lee Y, et al. Shh pathway activity is down-regulated in cultured medulloblastoma cells: implications for preclinical studies. *Cancer Res.* 2006;66(8):4215–4222.
38. AbuHammad SA-OX, Cullinane C, Martin C, et al. Regulation of PRMT5-MDM4 axis is critical in the response to CDK4/6 inhibitors in melanoma. *Proc Natl Acad Sci USA.* 2019;116(36):17990–18000. Erratum in: *Proc Natl Acad Sci USA.* 2020;117(17):9644–9645
39. Li Y, Chitnis N, Nakagawa H, et al. PRMT5 is required for lymphomagenesis triggered by multiple oncogenic drivers. *Cancer Discov.* 2015;5(3):288–303.
40. Taipale J, Chen JK, Cooper MK, et al. Effects of oncogenic mutations in Smoothened and Patched can be reversed by cyclopamine. *Nature.* 2000;406(6799):1005–1009.
41. Atwood SX, Sarin KY, Whitson RJ, et al. Smoothened variants explain the majority of drug resistance in basal cell carcinoma. *Cancer Cell.* 2015;27(3):342–353.